

High-resolution angle-resolved photoemission study of large magnetoresistance topological semimetal $CaAl_4$

Xu-Chuan Wu(吴徐传), Shen Xu(徐升), Jian-Feng Zhang(张建丰), Huan Ma(马欢), Kai Liu(刘凯), Tian-Long Xia(夏天龙), and Shan-Cai Wang(王善才)

Citation: Chin. Phys. B, 2021, 30 (**9**): 097303. DOI: 10.1088/1674-1056/ac0cd7
Journal homepage: http://cpb.iphy.ac.cn; http://iopscience.iop.org/cpb

What follows is a list of articles you may be interested in

Magneto-transport properties of thin flakes of Weyl semiconductor tellurium

Nan Zhang(张南), Bin Cheng(程斌), Hui Li(李惠), Lin Li(李林), and Chang-Gan Zeng(曾长淦)
Chin. Phys. B, 2021, 30 (**8**): 087304. DOI: 10.1088/1674-1056/ac0a5e

Tunneling magnetoresistance in ferromagnet/organic-ferromagnet/metal junctions

Yan-Qi Li(李彦琪), Hong-Jun Kan(阚洪君), Yuan-Yuan Miao(苗圆圆), Lei Yang(杨磊), Shuai Qiu(邱帅), Guang-Ping Zhang(张广平), Jun-Feng Ren(任俊峰), Chuan-Kui Wang(王传奎), Gui-Chao Hu(胡贵超)
Chin. Phys. B, 2020, 29 (**1**): 017303. DOI: 10.1088/1674-1056/ab5d02

Electrical spin polarization through spin-momentum locking in topological-insulator nanostructures

Minhao Zhang(张敏昊), Xuefeng Wang(王学锋), Fengqi Song(宋凤麒), Rong Zhang(张荣)
Chin. Phys. B, 2018, 27 (**9**): 097307. DOI: 10.1088/1674-1056/27/9/097307

Electronic transport properties of Co cluster-decorated graphene

Chao-Yi Cai(蔡超逸), Jian-Hao Chen(陈剑豪)
Chin. Phys. B, 2018, 27 (**6**): 067304. DOI: 10.1088/1674-1056/27/6/067304

Spin-valley-dependent transport and giant tunneling magnetoresistance in silicene with periodic electromagnetic modulations

Yi-Man Liu(刘一曼), Huai-Hua Shao(邵怀华), Guang-Hui Zhou(周光辉), Hong-Guang Piao(朴红光), Li-Qing Pan(潘礼庆), Min Liu(刘敏)
Chin. Phys. B, 2017, 26 (**12**): 127303. DOI: 10.1088/1674-1056/26/12/127303

High-resolution angle-resolved photoemission study of large magnetoresistance topological semimetal $CaAl_4$*

Xu-Chuan Wu(吴徐传)†, Shen Xu(徐升)†, Jian-Feng Zhang(张建丰)†, Huan Ma(马欢), Kai Liu(刘凯), Tian-Long Xia(夏天龙), and Shan-Cai Wang(王善才)‡

Department of Physics, Beijing Key Laboratory of Optoelectronic Functional Materials and Micro-nano Devices, Renmin University of China, Beijing 100872, *China*

(Received 19 April 2021; revised manuscript received 15 June 2021; accepted manuscript online 21 June 2021)

Extremely large magnetoresistance (XMR) has been explored in many nonmagnetic topologically nontrivial/trivial semimetals, while it is experimentally ambiguous which mechanism should be responsible in a specific material due to the complex electronic structures. In this paper, the magnetoresistance origin of single crystal $CaAl_4$ with $C2/m$ structure at low temperature is investigated, exhibiting unsaturated magnetoresistance of $\sim 3000\%$ at 2.5 K and 14 T as the fingerprints of XMR materials. By the combination of ARPES and the first-principles calculations, we elaborate multiband features and anisotropic Fermi surfaces, which can explain the mismatch of isotropic two-band model. Although the structural phase transition from $I4/mmm$ to $C2/m$ has been recognized, the subtle impact on electronic structure is revealed by our ARPES measurements. Considering that both charge compensation and potential topologically nontrivial band structure exist in $CaAl_4$, our findings report $CaAl_4$ as a new reference material for exploring the XMR phenomena.

Keywords: magnetoresistance, angle-resolved photoemission spectroscopy (ARPES), topological semimetal

PACS: 73.43.Qt, 79.60.−i **DOI:** 10.1088/1674-1056/ac0cd7

1. Introduction

The discovery of the extremely large magnetoresistance (XMR) in semimetal WTe_2[1] has attracted much attention to explore the origin of XMR. Magnetoresistance (MR) is the tendency for a material to change its electrical resistance in an externally applied magnetic field, which is widely used in spin devices, magnetic memory, and magnetic sensors. A series of materials with XMR have been found to exhibit very large unsaturated MR, meanwhile several effective mechanisms have been proposed to explain its origin. In electron–hole compensation mechanism,[2–8] the MR behavior changes quadratically with the magnetic field, written as $\mathrm{MR} = \mu_e\mu_h B^2$, where μ_e and μ_h are the mobilities of the electrons and holes, respectively. In semimetals with comparable carrier density, such as $PtBi_2$,[8,9] *TmPn* (*Tm* = Ta or Nb; *Pn* = N, P, As, Sb, Bi)[10–15] and YSb,[3] it can be explained by the carrier compensation mechanism well. The topological protection mechanism[16,17] can suppress the backscattering without magnetic field. The topological symmetry breaking can cause the XMR, in which the mobility of carries is highly dependent, such as Cd_3As_2,[18] TaAs family,[19] and ZrSiS family.[20–22] While other exotic mechanisms were proposed, open Fermi surfaces (FSs) have been observed in many XMR materials such as $MoAs_2$,[23] SiP_2,[24] and α-WP_2.[25] A field-induced change in the FSs was also reported to play a significant role in the origin of XMR.[26] XMR has been observed among a wide scope of materials, however, the underlying mechanism of XMR is not completely understood. The near-quadratic field dependence of MR and a field-induced up-turn followed by a resistivity plateau at low temperatures become their obvious fingerprints.

Recently, $CaAl_4$ with large unsaturated MR up to 3000% at 2.5 K and 14 T accompanied with a plateau was reported,[27] and similar magnetotransport fingerprints characterized by a near-quadratic field dependence of MR and field-induced up-turn in resistivity followed with a plateau at low temperature have also been observed. In this paper, by combining ARPES with the first-principles calculations and previous quantum oscillations,[27] we elaborate the topology of FSs and discuss the origin of the large MR in $CaAl_4$. Although structural phase transition from $I4/mmm$ to $C2/m$ has been recognized, the subtle impact on electronic structure is observed by our ARPES measurements. The measured and calculated FSs show multiband characters and anisotropic carrier pockets. Electrons and holes cannot compensate well in the fitting of previous transport data based on isotropic two-band model, while the calculated carrier density still supports the compensation mechanism. Moreover, the Z_2 invariant of $CaAl_4$ equals 1 and the band yields nontrivial Berry phase. The contribution of the topological band structure to MR needs further experi-

*Project supported by the National Natural Science Foundation of China (Grant Nos. 11774421, 12074425, 11874422, 11574391, and 11774424), the National Key Research and Development Program of China (Grant No. 2019YFA0308602), and the Fundamental Research Funds for the Central Universities, China, and the Research Funds of Renmin University of China (Grant Nos. 19XNLG13, 18XNLG14, and 19XNLG18).

†These authors contributed equally.

‡Corresponding author. E-mail: SCW@ruc.edu.cn

© 2021 Chinese Physical Society and IOP Publishing Ltd

mental investigation.

2. Experimental details

High-quality single crystals of $CaAl_4$ were grown by the flux method. ARPES measurements were performed at the beam line 13U of the National Synchrotron Radiation Laboratory (NSRL) at Hefei with a Scienta D80 analyser and the Kr discharge lamp ($h\upsilon = 10.05$ eV) with a Scienta R4000 analyser at Renmin University of China. The energy and angular resolutions were set as 15 meV and 0.05°, respectively. The samples were cleaved *in situ* along the (001) plane and measured at $T = 25$ K in a working vacuum better than 5×10^{-11} Torr. The first-principles electronic structure calculations on $CaAl_4$ were carried out with the projector augmented wave (PAW) method.[28,29] The generalized gradient approximation (GGA) of the Perdew–Burke–Ernzerhof (PBE) formula[30] for the exchange–correlation function was adopted. The kinetic energy cutoff of the plane-wave basis was set to be 350 eV. A $20 \times 20 \times 20$ k-point mesh was taken for the BZ sampling and the SOC effect was not considered. The lattice parameters and internal atomic positions were fully relaxed until the force on all atoms were smaller than 0.01 eV/Å. The FSs were calculated by performing the maximally localized Wannier functions (MLWF) method.[31,32]

3. Results

Figure 1(a) shows the schematic of $CaAl_4$'s crystal structure determined by the single crystal x-ray diffraction (XRD) pattern. The single crystal and powder XRD patterns can be well refined with $C2/m$ (No. 12) space group. The refined patterns yield the lattice parameters: $a = 6.1695$ Å, $b = 6.1842$ Å, $c = 6.3451$ Å, and $\beta = 118.05°$, which was reported in our previous results.[27] Another study suggests a transition at 443 K from $I4/mmm$ to $C2/m$ is a continuous process.[33] In addition, a second transformation might occur at $T \approx 243$ K, which is revealed by the specific heat and the elastic modulus.[34] Our temperature-dependent XRD measurement from 5 K to 300 K has been performed to rule out the possible phase transition.[27] Tetragonal $I4/mmm$ and monoclinic $C2/m$ own a fourfold rotation axis C_4 and a twofold rotation axis C_2, respectively. The electronic structures will be affected by the breaking of lattice symmetry, which will be further discussed in the ARPES measurement in detail. The cleavage plane oriented along the (001) direction is shown in Fig. 1(b). The 3D Brillouin zone (BZ) with high symmetry points and the top view of BZ are illustrated in Figs. 1(c) and 1(d), respectively.

Figure 2 demonstrates the high-resolution experimental contour intensity at $T = 25$ K and the corresponding Fermi surface from first-principles calculations. As shown in Figs. 2(a) and 2(b), the FS contour consists of a circular (α), four triangular (β) and a shuriken-like (γ) electron pockets centered at the Z points. Figure 2(b) plots the intensity maps at selected energies from E_F to -1.0 eV, and there are more bands at high binding energies. The top of the hole-like band is located at -0.75 eV. Below -0.5 eV, β pockets disappear and there is a square pocket which connects interior of the pocket γ. To display the distribution of FSs in reciprocal space intuitively, two clusters of FSs are shown in Figs. 2(c) and 2(d), respectively. The profile of the calculated FSs in Z-plane is almost identical to the measured FSs through ARPES measurements.

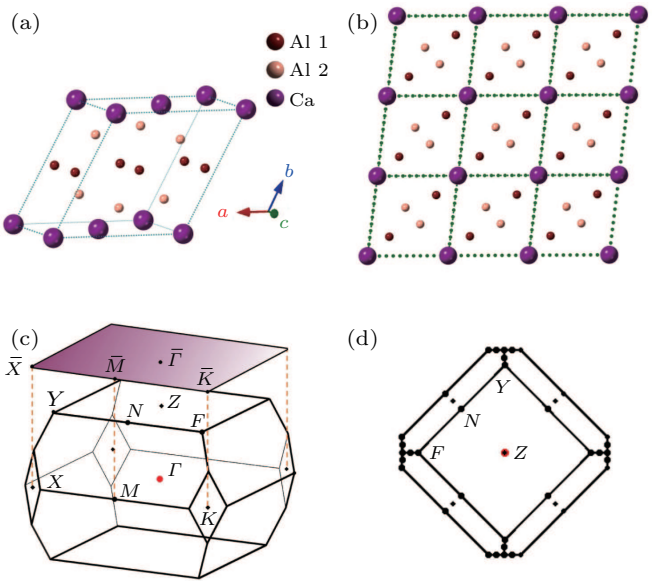


Fig. 1. Single crystal and Brillouin zone. (a) Crystal structure of $CaAl_4$ with space group $C2/m$ (No. 12). (b) The cleavage plane (001) of the crystal. (c) Schematic of the 3D first BZ and the (001)-projected surface BZ. (d) Top view of the 3D BZ.

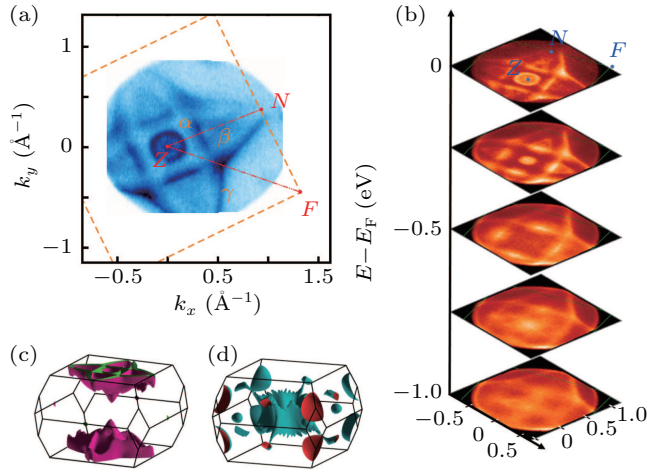


Fig. 2. ARPES band mapping and calculated FSs in $CaAl_4$. (a) Photoemission intensity map at the E_F in k_x–k_y plane at $T = 25$ K with $h\upsilon = 21$ eV, and the orange and red dashed lines indicate the 2D BZ boundary and the high-symmetry directions, respectively. (b) Photoemission intensity maps measured at energies from E_F to -1.0 eV. (c), (d) The calculated hole-like and electron-like 3D FSs of $CaAl_4$, respectively.

We have further verified the consistency between the experimental ARPES results (Figs. 3(a) and 3(b)) and the calculated band structures (Figs. 3(c) and 3(d)) along the high sym-

metry lines Z–N and Z–Y. The bands α, β, γ around Z can be clearly identified. A careful comparison between the DFT calculations and the ARPES intensity plots along high symmetry directions also reveals the high reliability of the calculations. Therefore it is reasonable to predict electronic transport properties by fitting the effective mass of the bands and calculating the volume of the FSs based on the first-principles calculations. It is noteworthy that a mini-band structure indicated by the red arrow (Fig. 4(f)) near the E_F cannot match any band in the bulk band calculations, and it can be also distinguished around Z in Fig. 4(e), which is possibly attributed to the contribution from the surface states.

Figure 4(a) illustrates the results of the FS mapping in the $k_{\|}$–k_z plane along the Γ–M (Z–N) direction. The intensity modulation of the band structures along k_z can be clearly observed. The angle-dependent SdH oscillation measurement indicates an ellipsoidal FS and a quasi-2D FS.[27] Band α is a circular pocket from the perspective of k_x–k_y plane. It is a narrow ellipse in $k_{\|}$–k_z plane and confirms that the FS of band α is an ellipsoid. The white dashed lines shown in Fig. 4(a) indicate the independent characteristic of k_z, which can also be verified in the calculated FS in Fig. 2(d). The spectral intensity of crossing band happens to exchange with the increase of photon energy as shown in Figs. 4(b)–4(d). It is consistent with the positions of two clusters of FSs (Figs. 2(c) and 2(d)) along the k_z direction.

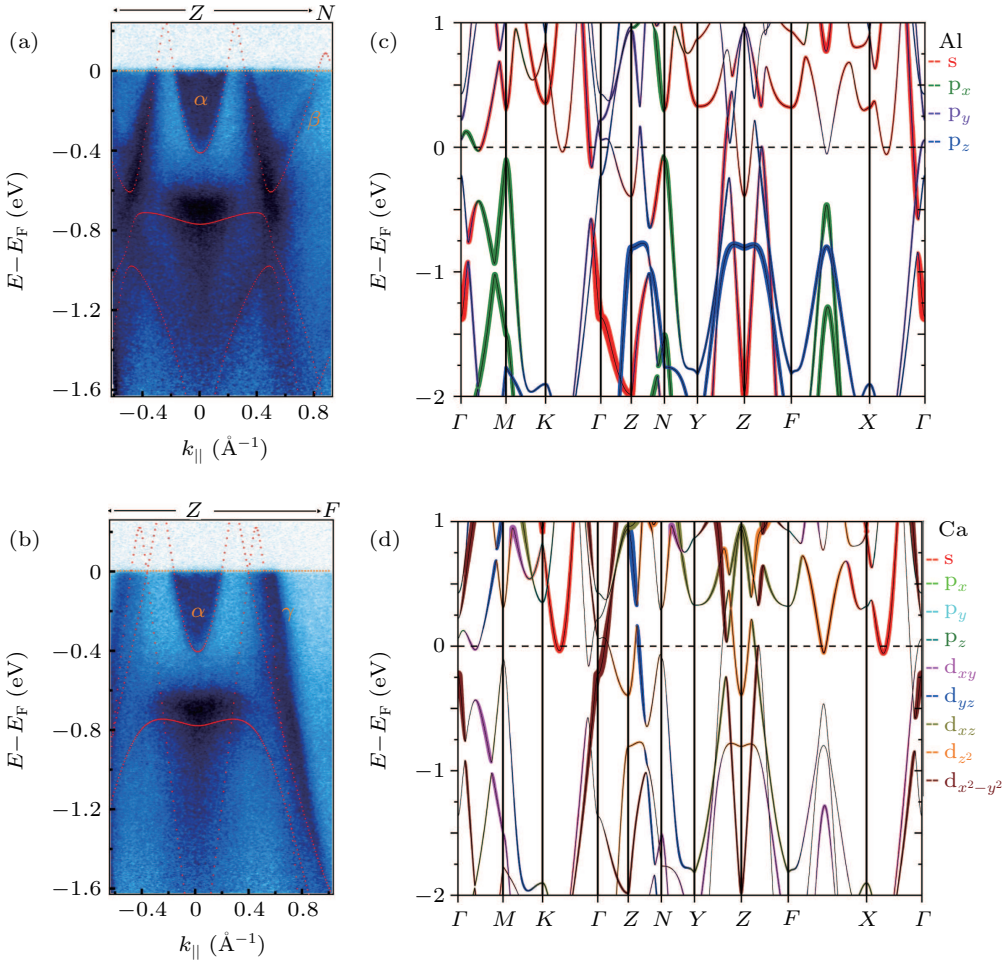


Fig. 3. (a), (b) The photoemission intensity plots along the high symmetry lines N–Z–N and F–Z–F, respectively. The red overlaid dashed lines in ARPES data indicate the DFT calculations. (c), (d) The calculated orbital-projected bulk band structures along the high symmetry lines without SOC.

4. Discussion

The symmetry of electronic structures is the reflection of crystal symmetry. Previous studies reported that a crystal structure transition from $I4/mmm$ to $C2/m$.[33] Two groups of ARPES intensity plots along the orthogonal high symmetry directions labelled Cut 1–4 (shown in Fig. 4(e)) verify the rotational symmetry of FSs. It is identical between two orthogonal directions within the resolution of the ARPES system that the locations and morphology of the bands (Figs. 4(f) and 4(g)) are observed. It is more likely that $CaAl_4$ has a quasi-C_4 rotational axis in its crystal structure, or it is in close proximity to C_4. The effective mass ratio $m^*_{\mathrm{Cut1}}/m^*_{\mathrm{Cut2}}$ fitted along the two directions Cut 1 and Cut 2 is ~ 0.98, indicated by the red markers extracted from the MDC analysis in Fig. 4(f). Consequently, it should be very careful to adjust the accuracy when simulating physical properties related to crystal symmetry.

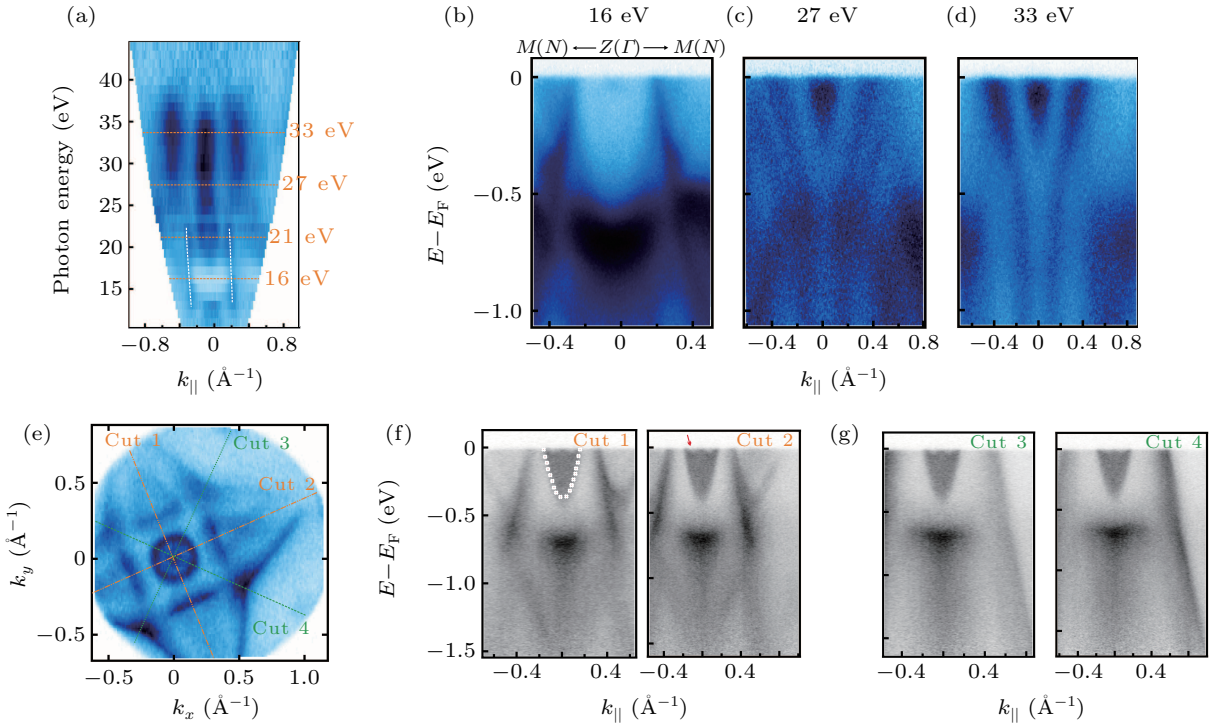


Fig. 4. (a) Photon energy dependent experimental FS mapping of $CaAl_4$. (b)–(d) The photoemission intensity plots along $M(N)$–$Z(\Gamma)$–$M(N)$ with photon energy $h\upsilon = 16$ eV, 27 eV, 33 eV, respectively. (e) Photoemission intensity map at the E_F in k_x–k_y plane at $T = 25$ K with $h\upsilon = 21$ eV. (f), (g) The photoemission intensity plots along two groups of high symmetry lines with $\pi/2$ angle, and corresponding directions are indicated by the orange and green dashed lines in (e).

It has been reported that $CaAl_4$ exhibited large unsaturated magnetoresistance $\sim 3000\%$ at 2.5 K and 14 T.[27] The observation of XMR in semimetals has triggered intensive research on the origin of XMR. An isotropic two-band model with perfect electron–hole compensation can lead to a quadratic dependence of magnetoresistance on magnetic field. To identify the specific values of the carriers in $CaAl_4$, a simplified two-band model has been developed to describe the Hall effect $\rho_{yx}(B)$ for the full temperature range

$$\rho_{yx}(B) = \frac{B}{e}\frac{\left(n_h\mu_h^2 - n_e\mu_e^2\right) + \left(n_h - n_e\right)\mu_e^2\mu_h^2B^2}{\left(n_h\mu_h + n_e\mu_e\right)^2 + \left[\left(n_h - n_e\right)\mu_e\mu_hB\right]^2}, \quad (1)$$

where $n_{e,h}$ and $\mu_{e,h}$ are the concentration and mobility of electrons and holes, respectively.[27] Fitting of the transport data at $T = 2.5$ K based on an over-simplified model yields that $n_e = 3.5 \times 10^{21}$ cm^{-3}, $n_h = 4.5 \times 10^{20}$ cm^{-3}, the mobility $\mu_e = 0.12$ m^2/V·s, and $\mu_h = 0.2$ m^2/V·s. The ratio of n_e/n_h at $T = 2.5$ K is approximately 7.8. which can explain the deviation $B^{1.6}$ field dependence. Luttinger's theorem states that the volume enclosed by the FSs is directly proportional to the particle density.[35,36] Due to the high consistency between the first-principles calculation and ARPES measurements, we can integrate the volume of the electron and hole pockets in reciprocal space, 0.1349 Å^{-3} and 0.1278 Å^{-3} for electron and hole pockets, respectively. The ratio of n_e/n_h from the calculation is approximately compensated. Therefore, we need to discuss whether the carrier concentration obtained by the MR fitting based on two-band model is reasonable. Such an imbalanced charge carrier densities fitting from the isotropic two-band model results in a saturating MR curve at intermediate magnetic field, unless a large distinction between the electron and hole mobility is considered for the fitting process.[3] However, it is contradictory that unsaturated MR up to 3000% at 2.5 K was observed in $CaAl_4$.[27] The nonlinear Hall resistivity, angle-dependent SdH quantum oscillation experiments, and the DFT calculations indicate multiband feature and strong anisotropy of FSs.[27] Different orbitals from Ca and Al atoms go through the E_F to form the complex FSs, shown in Figs. 3(c)–3(d). As discussed before, an isotropic two-band model typically assumes uniform mobility in all directions for each type of carriers. Apparently, this assumption on the mobility is not rational, where the anisotropic FS has been shown in ARPES measurements and calculated FSs. It is necessary to consider the anisotropic multiband nature of $CaAl_4$ in a quantitative MR analysis.

To further explore the origin of large MR, possible topological protection in $CaAl_4$ is discussed by combing the ARPES with Z_2 invariant and Landau fan diagram of Landau level (LL) index yielding Berry phase (ϕ_B) in our previous work.[27] The extreme cross section of FS, angular dependence of the SdH peak,[27] and the calculated 3D FS in Fig. 2(c) jointly confirm the existence of band α shown in Fig. 2(a). The LL index of band α is approaching to a nontrivial Berry phase of 0.93π.[27] Moreover, there are both time-reversal and space-inversion symmetries in $CaAl_4$ with $C2/m$. The topological invariant Z_2 of $CaAl_4$ equals 1, which is calculated

from the product of the parities of all the occupied bands at the eight time-reversal invariant momentum (TRIM) points.[27] We have not found the expected topologically nontrivial surface state and band crossing. Thus it is worth studying further to learn more about the topological protection mechanism.

5. Conclusion

In summary, we perform APRES measurements and carry out first-principles calculations to comprehensively describe the electronic structure of $CaAl_4$. A subtle impact from the structural phase transition from $I4/mmm$ to $C2/m$ is observed. A quasi-2D FS can be confirmed by the k_z-dependent ARPES and the calculated FSs. The origin of large MR in $CaAl_4$ is mostly attributed to the electron–hole compensation mechanism and topologically nontrivial electronic structures. Multiband features and the anisotropic FSs revealed by the ARPES measurements, the first-principles calculations and magneto-transport properties reveal the discrepancy of the carrier density ratio n_e/n_h between the isotropic two-band model and Luttinger's theorem. Thus, a general multiple-band model and further ARPES measurements should be considered to explore the perfect compensation and electronic band topology.

Acknowledgment

The authors thank the technical assistance from the BL13U beamline in National Synchrotron Radiation Laboratory (NSRL).

References

[1] Soluyanov A A, Gresch D, Wang Z, Wu Q, Troyer M, Dai X and Bernevig B A 2015 *Nature* **527** 495
[2] Zeng L K, Lou R, Wu D S, Xu Q N, Guo P J, Kong L Y, Zhong Y G, Ma J Z, Fu B B, Richard P, Wang P, Liu G T, Lu L, Huang Y B, Fang C, Sun S S, Wang Q, Wang L, Shi Y G, Weng H M, Lei H C, Liu K, Wang S C, Qian T, Luo J L and Ding H 2016 *Phys. Rev. Lett.* **117** 127204
[3] Xu J, Ghimire N J, Jiang J S, Xiao Z L, Botana A S, Wang Y L, Hao Y, Pearson J E and Kwok W K 2017 *Phys. Rev. B* **96** 075159
[4] He J, Zhang C, Ghimire N J, Liang T, Jia C, Jiang J, Tang S, Chen S, He Y, Mo S K, Hwang C C, Hashimoto M, Lu D H, Moritz B, Devereaux T P, Chen Y L, Mitchell J F and Shen Z X 2016 *Phys. Rev. Lett.* **117** 267201
[5] Shekhar C, Nayak A K, Sun Y, Schmidt M, Nicklas M, Leermakers I, Zeitler U, Skourski Y, Wosnitza J, Liu Z K, Chen Y L, Schnelle W, Borrmann H, Grin Y, Felser C and Yan B H 2015 *Nat. Phys.* **11** 645
[6] Ghimire N J, Botana A S, Phelan D, Zheng H and Mitchell J F 2016 *J. Phys. Condens. Matter* **28** 235601
[7] Zhu Z, Lin X, Liu J, Fauque B, Tao Q, Yang C, Shi Y and Behnia K 2015 *Phys. Rev. Lett.* **114** 176601
[8] Gao W, Hao N, Zheng F W, Ning W, Wu M, Zhu X, Zheng G, Zhang J, Lu J, Zhang H, Xi C, Yang J, Du H, Zhang P, Zhang Y and Tian M 2017 *Phys. Rev. Lett.* **118** 256601
[9] Yao Q, Du Y P, Yang X J, Zheng Y, Xu D F, Niu X H, Shen X P, Yang H F, Dudin P, Kim T K, Hoesch M, Vobornik I, Xu Z A, Wan X G, Feng D L and Shen D W 2016 *Phys. Rev. B* **94** 235140
[10] Li Y K, Li L, Wang J L, Wang T T, Xu X F, Xi C Y, Cao C and Dai J H 2016 *Phys. Rev. B* **94** 121115
[11] Luo Y, McDonald R D, Rosa P F, Scott B, Wakeham N, Ghimire N J, Bauer E D, Thompson J D and Ronning F 2016 *Sci. Rep.* **6** 27294
[12] Shen B, Deng X Y, Kotliar G and Ni N 2016 *Phys. Rev. B* **93** 195119
[13] Yuan Z J, Lu H, Liu Y J, Wang J F and Jia S 2016 *Phys. Rev. B* **93** 184405
[14] Wu D S, Liao J, Yi W, Wang X, Li P G, Weng H M, Shi Y G, Li Y Q, Luo J L, Dai X and Fang Z 2016 *Appl. Phys. Lett.* **108** 494024
[15] Wang Y Y, Yu Q H, Guo P J, Liu K and Xia T L 2016 *Phys. Rev. B* **94** 041103
[16] Wang Y Y, Yu Q H and Xia T L 2016 *Chin. Phys. B* **25** 107503
[17] Jing Y M, Huang S Y, Wu J X, Peng H L and Xu H Q 2018 *Acta. Phys. Sin.* **67** 047301 (in Chinese)
[18] Liang T, Gibson Q, Ali M N, Liu M, Cava R J and Ong N P 2015 *Nat. Mater.* **14** 280
[19] Huang X C, Zhao L X, Long Y J, Wang P P, Chen D, Yang Z H, Liang H, Xue M Q, Weng H M, Fang Z, Dai X and Chen G F 2015 *Phys. Rev. X* **5** 031023
[20] Xu Q N, Song Z D, Nie S M, Weng H M, Fang Z and Dai X 2015 *Phys. Rev. B* **92** 205310
[21] Kumar N, Manna K, Qi Y, Wu S C, Wang L, Yan B, Felser C and Shekhar C 2017 *Phys. Rev. B* **95** 121109
[22] Hu J, Tang Z, Liu J, Liu X, Zhu Y, Graf D, Myhro K, Tran S, Lau C N, Wei J and Mao Z 2016 *Phys. Rev. Lett.* **117** 016602
[23] Lou R, Xu Y F, Zhao L X, Han Z Q, Guo P J, Li M, Wang J C, Fu B B, Liu Z H, Huang Y B, Richard P, Qian T, Liu K, Chen G F, Weng H M, Ding H and Wang S C 2017 *Phys. Rev. B* **96** 241106
[24] Zhou Y X, Lou Z F, Zhang S N, Chen H C, Chen Q, Xu B J, Du J H, Yang J H, Wang H D, Xi C Y, Pi L, Wu Q S, Yazyev O V and Fang M H 2020 *Phys. Rev. B* **102** 115145
[25] Du J H, Lou Z F, Zhang S N, Zhou Y X, Xu B J, Chen Q, Tang Y Q, Chen S J, Chen H C, Zhu Q Q, Wang H D, Yang J H, Wu Q S, Yazyev O V and Fang M H 2018 *Phys. Rev. B* **97** 245101
[26] Wang K, Graf D, Li L, Wang L and Petrovic C 2014 *Sci. Rep.* **4** 7328
[27] Xu S, Zhang J F, Wang Y Y, Sun L L, Wang H, Su Y, Wang X Y, Liu K and Xia T L 2019 *Phys. Rev. B* **99** 115138
[28] Blochl P E 1994 *Phys. Rev. B* **50** 17953
[29] Kresse G and Joubert D 1999 *Phys. Rev. B* **59** 1758
[30] Perdew J P, Burke K and Ernzerhof M 1996 *Phys. Rev. Lett.* **77** 3865
[31] Souza I, Marzari N and Vanderbilt D 2001 *Phys. Rev. B* **65** 035109
[32] Marzari N and Vanderbilt D 1997 *Phys. Rev. B* **56** 12847
[33] Miller G J, Li F and Franzen H F 1993 *J. Am. Chem. Soc.* **115** 3739
[34] Zogg H and Schwellinger P 1979 *J. Mater. Sci.* **14** 1923
[35] Luttinger J M 1960 *Phys. Rev.* **119** 1153
[36] Luttinger J M and Ward J C 1960 *Phys. Rev.* **118** 1417